water

MDPI

Article

New Compound Open Channel Section with Polynomial Sides: Improving Cost and Aesthetics

Said M. Easa [1,*] and Yan-Cheng Han [2]

1 Department of Civil Engineering, Ryerson University, Toronto, ON M5B 2K3, Canada
2 Department of Hydraulic Engineering, School of Resources and Environment, University of Jinan, Jinan 250022, China
* Correspondence: seasa@ryerson.ca

Received: 6 May 2019; Accepted: 20 July 2019; Published: 25 July 2019

Abstract: Previous research on compound trapezoidal cross sections has mainly focused on improving the prediction of the discharge (flow rate) because of its inherent challenges. This paper focuses on two other important aspects: Section shape and optimal construction cost. First, the paper proposes a new compound section with third-degree polynomial sides of main channel with horizontal bottom (HB) that allows its top corners to be smooth, called herein compound polynomial section. The special cases of this versatile section include the simple polynomial section, polygonal section, trapezoidal-rectangular section, two-segment linear-side section, and parabolic bottom-trapezoidal section. The simple polynomial section, which is the bank-full part of the compound polynomial section, can further produce parabolic (with or without HB), trapezoidal, rectangular, and triangular sections. Second, an optimization model that minimizes construction cost (excavation and lining) of the compound (or simple) polynomial section is developed. The model includes discharge and physical constraints. Theoretical and empirical methods of discharge prediction were used in the model. The results show that the simple polynomial section was more economical than the popular parabolic section by up to 8.6% when the side slopes were restricted. The new polynomial-based sections not only reduced construction cost, but also improved maintenance and aesthetics. As such, the new sections should be of interest to researchers and practitioners in hydraulic engineering.

Keywords: compound; cross section; polynomial sides; smooth corners; construction cost; horizontal bottom; optimization

1. Introduction

Many types of open channel cross sections have been developed over the years to improve construction cost and hydraulic efficiency, and to provide the users with flexibility in accommodating physical constraints. Open channel sections can be classified into three families [1]: Linear family (only linear segments), curved family (only curved segments), and linear-curved family (combined linear and curved segments). The development of these sections started with conventional sections, followed by inspiring sections, and continued with more new recent sections (Table 1). To put the research of this study in perspective, it is useful to present a brief description of these section families.

The linear family includes trapezoidal, rectangular, triangular, and compound. The characteristics of the trapezoidal section and its special cases (rectangular and triangular) are well documented in the literature [2–4]. The optimal design of these sections has been addressed by numerous researchers, including Swamee [5], Guo and Hughes [6], Das [7], Jain and Bhattacharjya [8], Aksoy and Altan-Sakarya [9], Han et al. [10], and Froehlich [11]. The curved family includes parabolic, power-law, catenary, circular, and horseshoe. The most popular in this family is the parabolic section whose optimal characteristics have been addressed by numerous authors, including Mironenko et al. [12], Loganathan [13], Chahar and Ahmed [14], Hussein [15] Strelkoff and Clemmens [16], Anwar and Clarke [17], and Anwar and de Vries [18]. The horseshoe, egg-shaped, and circular sections have been used in the sewerage systems, particularly combined systems, for more than a century, see Carson et al. [19]. However, current systems use mainly circular sections and tend to be separate. The closed non-circular sections were developed mostly for combined systems, basically due to the great discrepancy between sanitary and stormwater flow rates. These systems are being replaced with separate systems using circular sections due mainly to the need of wastewater treatment, see Diogo et al. [20].

Table 1. Historical developments of the main shapes of open channel sections.

Section Designation	Section Family	Section Type [1]	Reference	Year
Conventional	Linear	Trapezoidal, rectangular	Chow [4]	1959
	Linear	Compound	Chow [4]	1959
	Curved	Circular, Parabolic	Chow [4]	1959
	Curved	Horseshoe	Carson et al. [19]	1894
	Curved	Power-law	Strelkoff and Clemmens [16]	2000
	Linear-curved	P-bottom trapezoidal	Babaeyan et al. [21]	2000
	Linear-curved	C-bottom trapezoidal	Chahar and Basu [22]	2009
Inspiring Initiatives	Linear	Polygonal	Kurbanov and Khanov [23]	2003
	Linear	Trapezoidal-rectangular	Abdulrahman [24]	2007
	Linear-curved	HB-PS	Das [25]	2007
	Linear-curved	Trapezoidal-RC	Froehlich [26]	2008
	Linear-curved	TSPS-HB	Easa [27]	2009
Recent Developments	Linear	TSLS-HB	Vatankhah [28]	2010
	Linear	MSLS-HB	Easa [29]	2011
	Linear-curved	Standard ES-HB	Easa and Vatankhah [30]	2014
	Linear-curved	General ES-HB	Easa [31]	2016
	Curved	Cubic parabolic sides	Han and Easa [32]	2017
	Curved	Super PL	Han and Easa [33]	2018

[1] C = circular, ES = elliptic sides, HB = horizontal bottom, MSPS = multi-segment linear sides, P = parabolic, PL = power-law, PS = parabolic sides, RC = round corners, TSPS = two-segment parabolic sides, TSLS = two-segment linear sides.

The linear-curved family includes parabolic-bottom trapezoidal, circular-bottom trapezoidal, round-corner rectangle, and pipe-handle sections, which is normally used in the sewer system. The round corners at the bottom of the rectangular section help improve maintenance. Limited research has been conducted for the sections of this family, see Babaeyan-Koopaei et al. [21] and Chahra and Basu [22].

During the period (2003–2009), a few authors started to modify the conventional shapes of channel sections. The new sections included polygonal section by Kurbanov and Khanov [23], trapezoidal-rectangular section by Abdulrahman [24], parabolic sides with horizontal bottom (HB) by Das [25], trapezoidal section with round corners by Froehlich [26], and two-segment parabolic sides with HB by Easa [27]. These sections have subsequently inspired the development of more new sections (2010–2018), such as semi-regular polygon by Vatankhah [28], multiple-segment linear sides by Easa [29], standard elliptic sides by Easa and Vatankhah [30], general elliptic side by Easa [31], and cubic and power-law (PL) sections by Han and Easa [32,33]. As noted, the trend of recent advances in section shape has been to introduce additional linear or curved elements, such as HB and round bottom corners, to improve discharge (flow rate) and maintenance.

Among the preceding sections, the compound section has presented a challenge to researchers regarding how to estimate its discharge accurately. Considerable research has been conducted to improve the prediction accuracy of the discharge, as will be discussed in the next section. However, to the authors' knowledge, the optimal characteristics of this section have not been addressed in the literature. In addition, unlike the trapezoidal section, the shape of the compound section remains linear. Better geometric (linear-curved) shapes of this section can be easily analyzed, given the advances in mathematical optimization and computer technology. This paper presents two main research contributions to compound sections. First, a new curved shape of the sides of the main channel of the compound section that have smooth top corners is modeled using a third-degree polynomial. The new section, called herein the compound polynomial section, is versatile and can produce many sections as special cases, including the simple polynomial section (bank-full part), polygonal section, trapezoidal-rectangular section, two-segment linear-side section, and parabolic bottom-trapezoidal section. In addition, the simple polynomial section can produce the trapezoidal, rectangular, triangular, and parabolic sections. Second, an optimization model that minimizes the construction cost of the compound (or simple) polynomial section is presented. Besides improving maintenance and aesthetics, the simple polynomial section was found to be more economical than the popular parabolic section. Due to the challenge in accurately estimating the discharge of the compound section (which is required by the optimization model), various discharge methods were reviewed.

The next section reviews various methods of discharge prediction for compound sections. The following section presents the geometric and hydraulic characteristics of the proposed compound and simple polynomial sections, and conditions for special cases. The optimization model of the most economic compound (or simple) polynomial section and application of the model are then presented, followed by the conclusions.

2. Review of Discharge Methods

2.1. General

Prediction of the true discharge of the compound section has been a challenge. Numerous analytical methods have been developed to improve the accuracy of estimating the discharge, including Posey [34], Shiono and Knight [35], Wark et al. [36], Ackers [37], Wormleaton and Merrett [38], Lambert and Myers [39], Bousmar and Zech [40], and Ervine et al. [41]. Other methods based on nonlinear regression analysis and artificial neural networks were developed by MacLeod [42], Liu and James [43], Zahiri and Dehghani [44], and Unal et al. [45]. To further improve prediction accuracy and reduce the extensive computations required by some methods, general empirical methods have been recently developed by Azamathulla and Zahiri [46] and Hosseini [47]. The empirical methods use field and laboratory experiments to develop revised formulas of the discharge of the compound section to improve prediction accuracy. The methods of discharge prediction for compound sections are divided here into two categories: Theoretical methods and empirical methods.

2.2. Theoretical Methods

The theoretical methods rely on developing better formulas for the composite Manning roughness coefficient of the compound section. Several methods have been proposed by researchers and have produced substantially different results. In these methods, the coefficient is calculated based on different assumptions regarding the relationship between the subsections with respect to discharges, velocities, shear stresses, and forces. One of the widely used theoretical methods (conventional method) assumes that the total discharge equals the sum of subsection discharges. The compound section is simply divided into several subsections. Different ways can be used to divide the section. The vertical division is adopted here as it is the basis for the empirical discharge prediction method used in the proposed optimization model (Figure 1). Then, based on this divided channel method (DCM), the discharge is calculated as the sum of subsection discharges, as follows [4].

$$Q_{DCM} = \sum_{i=1}^{N} Q_i = \sum_{i=1}^{N} \left(\frac{A_i^{5/3} S_o^{1/2}}{n_i P_i^{2/3}} \right) \text{ (DCM)} \tag{1}$$

where Q_{DCM} = total discharge of the compound section using DCM (m^3/s), N = number of subsections of the compound section, Q_i = discharge of Subsection i (m^3/s), A_i = flow area of Subsection i (m^2),

S_o = longitudinal bed slope (m/m), n_i = Manning roughness coefficient of Subsection i, and P_i = wetted perimeter of Subsection i (m).

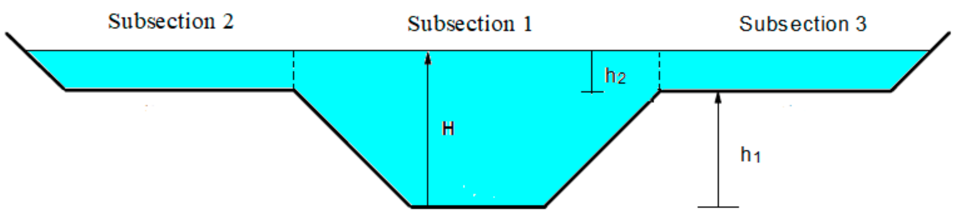

Figure 1. Division of typical compound section by vertical lines.

The conventional method ignores the shear stress at the interfaces of the subsections and therefore may overestimate the discharge. In a recent laboratory experiment by Fernandes et al. [48], the difference between the DCM-computed and measured discharges was up to 7% and 32%, respectively, for constant roughness and rougher floodplains with relatively small water depths.

Since each subsection generally has different roughness coefficients, frequently with the upper subsection rougher, the equivalent Manning's roughness coefficient proposed by Horton [49] is used,

$$n_e = \left[\frac{\sum_{j=1}^{m} \left(P_j n_j^{1.5} \right)}{P} \right]^{2/3} \tag{2}$$

where m = number of wetted elements in the subsection (m = 3 in Subsection 1 and m = 2 in Subsection 2 or 3), P_j = length of element j of the subsection, n_j = roughness coefficient of element j of the subsection, and P = wetted perimeter of the subsection. It should be noted that Equation (2) assumes that all subsections have the same average velocity, which may be a coarse approximation. In addition, the types and sources of the errors and their components do not seem to be fully known.

McAtee [50] evaluated seven theoretical methods for computing the composite roughness of compound channels, n_c, and found that the largest discharge of these methods was 35% greater than the smallest discharge. However, the author cited two studies, one by Motayed and Krishnamurthy [51] who used data from 36 gauged streams in four states to test four different methods for calculating n_c. They found that the mean error between the computed and measured n_c was the smallest for the Lotter method. Another study in 2007 by Yang et al. [52] that used a single artificial composite compound channel at 50 different discharge rates also found that the mean relative error for n_c was smallest for the Lotter method.

The Lotter method assumes that the total discharge equals the sum of the three subsection discharges. As such, it is identical to the DCM of Equation (1). Based on the preceding studies, the Lotter method (DCM) is used, along with the empirical methods, in the proposed optimization model for compound sections. Note that even though these methods may produce very different results, the preceding studies [51,52] indicate that other theoretical methods are clearly worse than the DCM.

2.3. Empirical Methods

2.3.1. Azamathulla and Zahiri Method (2012)

Azamathulla and Zahiri [46] developed a precise dimensionless model for estimating the flow discharge of a compound section using linear genetic optimization. The model was calibrated using published stage–discharge data for 394 laboratories and field data for 30 compound channels.

The discharge ratio in the compound section (total discharge to bank-full discharge) was developed as a function of dimensionless variables. The formula of the total discharge can be written as:

$$Q_{E-AZ} = 1.496\, Q_b \left(\frac{Q_{DCM}}{Q_b}\right)^{0.8642 D_r} (1 - \ coh)^{-0.1687} D_r^{0.214} \tag{3}$$

where Q_{E-AZ} = discharge of the compound section based on the empirical Azamathulla and Zahiri (E-AZ) method (m^3/s), Q_b = bank-full discharge (m^3/s), coh = coherence variable of the compound section, and D_r = ratio of water depth in the floodplain to that in the main channel. The coefficient of determination, r^2, of Equation (3) is 0.951.

The coherence variable coh is defined as the ratio of the conveyance of the compound section as a single unit to that based on the conventional DCM. That is,

$$coh = \frac{\dfrac{A_c^{5/3}}{\left(\sum_{i=1}^{N} n_i^{1.5}\ P_i\right)^{2/3}}}{\sum_{i=1}^{N}\left(\dfrac{A_i^{5/3}}{n_i P_i^{2/3}}\right)} \tag{4}$$

2.3.2. Hosseini Method (2004)

Hosseini [47] used experimental data from a United Kingdom flood channel facility to develop adjustment coefficients for the DCM subsection discharges. The total adjusted discharge is then given by:

$$Q_{E-H} = uQ_1 + v(Q_1 + Q_2) \tag{5}$$

where Q_{E-H} = total discharge of the compound section based on the empirical Hosseini (E-H) method (m^3/s), u, v = adjustment coefficients for the DCM discharges of the main channel and floodplain subsections, respectively, and Q_1, Q_2, Q_3 = DCM discharges of Subsections 1–3, respectively (m^3/s). The adjustment coefficients are given by:

$$u = 0.782 \left(\frac{h_2}{H}\right)^{-0.128} coh^{0.353} \tag{6}$$

$$v = 0.903 \left(\frac{h_2}{H}\right)^{-0.197} coh^{0.547} \tag{7}$$

where H = water depth in the main channel (m) and h_2 = water depth in the floodplain (m). The values of r^2 of Equations (6) and (7) are 0.999 and 0.998, respectively.

3. Proposed Polynomial Sections

3.1. Compound Polynomial Section

3.1.1. Section Geometry

The compound section consists of the main channel and the floodplain. For the purpose of calculating the discharge, the compound section can be divided into subsections in different ways using horizontal, vertical, or inclined dividing lines [50]. However, since the discharge constraint used in the proposed optimization model is based on a vertical division, this division scheme was implemented to maintain consistency in the entire model. The compound section is divided into three subsections using two vertical lines (Figure 2). Subsection 1 is the main channel, subsection 2 is the left floodplain, and subsection 3 is the right floodplain. Subsection 1 has a HB width b_1. Subsection 2 has a horizontal bank width b_2, while that of subsection 3 is b_3. Both subsections 2 and 3 have inverse side slope z_2, water depth h_2, and freeboard f_2 (vertical distance). For the compound section, the water surface width is T_2 and the section width at the ground level is T_{2f}. To make the model more general, different Manning roughness coefficients were assumed for the HB of the main section (n_1), main section sides (n_2), floodplain bank (n_3), and floodplain sides (n_4), as shown in Figure 2.

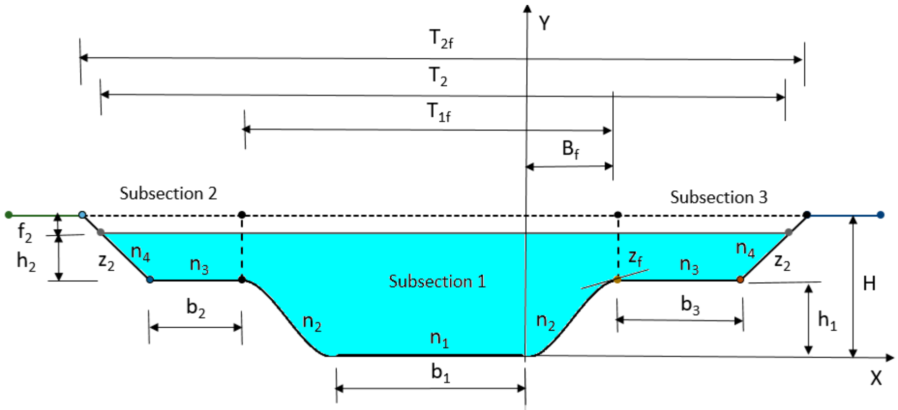

Figure 2. Proposed compound section with polynomial sides for main channel.

3.1.2. Polynomial Side Characteristics

Consider Cartesian coordinate axes with an origin at the right end of the HB, where the x-axis is along the HB. The sides of the main channel section are represented by the following third-degree polynomial:

$$y = bx + cx^2 + dx^3 \tag{8}$$

where b, c, d = parameters to be determined by optimization. The first derivative of y with respect to x of Equation (8), y', is given by:

$$y' = b + 2cx + 3dx^2 \tag{9}$$

Let the inverse side slope at the ground level be z_f (horizontal to vertical distances) and B_f be the horizontal distance from the y-axis to the top point of the main channel side. Then, when $x = B_f$, $y' = 1/z_f$. Solving Equation (9) for B_f gives:

$$B_f = \begin{cases} \dfrac{-2c \pm \sqrt{4c^2 - 12d\left(b - \frac{1}{z_f}\right)}}{6d}, & \text{for } d \neq 0 \\ \dfrac{\frac{1}{z_f} - b}{2c}, & \text{for } d = 0 \end{cases} \tag{10}$$

To ensure that the radical in Equation (10) is positive, the following condition applies:

$$z_f \begin{cases} \leq \dfrac{3d}{3bd - c^2}, & \text{for } \left(3bd - c^2\right) > 0 \text{ and } d > 0 \\ \geq \dfrac{3d}{3bd - c^2}, & \text{for } \left(3bd - c^2\right) < 0 \text{ and } d < 0 \end{cases} \tag{11}$$

Other conditions are used to ensure a feasible geometry of the compound section (e.g., $z_f \geq 0$). Then, the bank-full water depth h_1 is given by:

$$h_1 = bB_f + cB_f^2 + dB_f^3 \tag{12}$$

The total width at the bank level, T_{1f} is given by:

$$T_{1f} = b_1 + 2B_f \tag{13}$$

where b_1 = width of the HB of the main channel.

3.1.3. Subsection Characteristics

For subsection 1, the flow area A_1 and the wetted perimeter P_1 are easily calculated. That is,

$$A_1 = A_{main\ f} + h_2 T_{1f} \tag{14}$$

$$P_1 = b_1 + 2P_{sf} \tag{15}$$

where $A_{main\ f}$ = bank-full flow area of subsection 1 and P_{sf} = length of the total side of subsection 1. The area $A_{main\ f}$ is given by:

$$A_{main\ f} = \left(b_1 + 2B_f\right)h_1 - 2\int_0^{B_f} y dx = \left(b_1 + 2B_f\right)h_1 - 2\left(\frac{bB_f^2}{2} + \frac{cB_f^3}{3} + \frac{dB_f^4}{4}\right) \tag{16}$$

The length P_{sf} is given by:

$$P_{sf} = \int_0^{B_f} \sqrt{1 + (dy/dx)^2} dx \tag{17}$$

Substituting for the first derivative of y from Equation (9) into Equation (17), then:

$$P_{sf} = \int_0^{B_f} \sqrt{1 + (b + 2\,cx + 3\,dx^2)^2} dx \tag{18}$$

The integral of Equation (18) can be approximated using the three-point Gauss-quadrature method as:

$$\begin{aligned} P_{sf} = \tfrac{B_f}{18}\Bigg\{ & 5\sqrt{1 + \left[b + 1.7746\,cB_f + 2.3619\,dB_f^2\right]^2} \\ & + 5\sqrt{1 + \left[b + 0.2254cB_f + 0.0381dB_f^2\right]^2} \\ & +8\sqrt{1 + \left[b + cB_f + 0.75\,dB_f^2\right]^2}\Bigg\} \end{aligned} \tag{19}$$

For subsection 2, the flow area A_2 and the wetted perimeter P_2 are given by:

$$A_2 = h_2\left(b_2 + \frac{h_2\,z_2}{2}\right) \tag{20}$$

$$P_2 = b_2 + h_2\sqrt{1 + z_2^2} \tag{21}$$

Similarly, for subsection 3, the flow area A_3 and the wetted perimeter P_3 are given by:

$$A_3 = h_2\left(b_3 + \frac{h_2\,z_2}{2}\right) \tag{22}$$

$$P_3 = b_3 + h_2\sqrt{1 + z_2^2} \tag{23}$$

For the compound section, the water surface width T_2 and the ground surface width T_{2f} are given by:

$$T_2 = T_{1f} + b_2 + b_3 + 2z_2 h_2 \tag{24}$$

$$T_{2f} = T_2 + 2z_2 f_2 \tag{25}$$

For construction cost, the total areas of subsections 2 and 3 and their side lengths are given by:

$$A_{1f} = A_1 + T_{1f} f_2 \tag{26}$$

$$A_{2f} = A_2 + b_2 f_2 + \frac{f_2 z_2 (f_2 + 2h_2)}{2} \tag{27}$$

$$A_{3f} = A_3 + b_3 f_2 + \frac{f_2 z_2 (f_2 + 2h_2)}{2} \tag{28}$$

$$P_{2sf} = P_{3sf} = (h_2 + f_2)\sqrt{1 + z_2^2} \tag{29}$$

where A_{1f} = total area of subsection 1, A_{2f} = total area of subsection 2, A_{3f} = total area of subsection 3, and P_{2sf} , P_{3sf} = lengths of the side of subsections 2 and 3, respectively.

3.2. Simple Polynomial Section

The bank-full part of the main channel (no floodplains) is a special case of the compound section and can be designed and implemented in its own. The simple polynomial section has HB width b_1 and third-degree polynomial sides (Figure 3). The inverse side slope at the bank level is z_f, where the x and y coordinates are B_f and h_1, respectively. The water surface width is T_1 and the width at the bank level is T_{1f}.

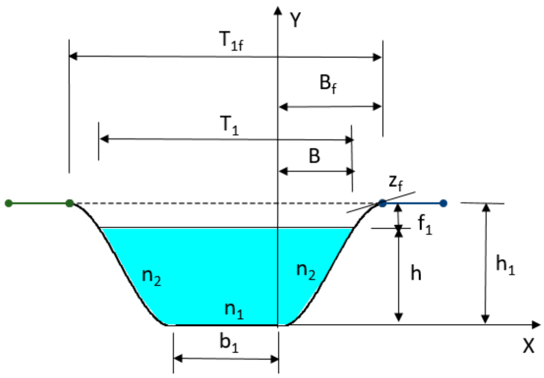

Figure 3. Simple polynomial section.

The flow depth of the simple polynomial section h is calculated as $(h_1 - f_1)$. Let B be the distance along the water surface from the y-axis to section side. Since $x = B$ when $y = h$, substituting these values in Equation (8) and solving the cubic equation for B gives:

$$B = 2\sqrt{-K}\cos\left(\frac{\theta}{3} + 240^{\circ}\right) - \frac{c}{3\,d} \tag{30}$$

where:

$$\theta = \cos^{-1}\left(\frac{R}{\sqrt{-K^3}}\right) \tag{31}$$

$$K = \frac{3\left(\frac{b}{d}\right) - \left(\frac{c}{d}\right)^2}{9} \tag{32}$$

$$R = \frac{9\left(\frac{c}{d}\right)\left(\frac{b}{d}\right) + 27h - 2\left(\frac{c}{d}\right)^3}{54} \tag{33}$$

For the special case of parabolic sides ($b = d = 0$), $B = (h/c)^{1/2}$.

The flow area and wetted perimeter of the simple polynomial section are denoted by A_{main} and P_{main}. The flow area is calculated similarly using Equation (16) after replacing B_f with B. The wetted perimeter $P_{main} = b_1 + 2P_s$, where P_s = length of the wetted side, which is calculated similarly using Equation (19) after replacing B_f with B. The water surface width is given by $T_1 = b_1 + 2B$.

For construction cost, the total section area equals $A_{main\ f}$ of Equation (16) and the total length of the side is P_{sf} of Equation (19).

3.3. Special Cases

The special cases of the compound and simple polynomial sections are shown in Table 2. As noted, beside the simple polynomial section, the compound polynomial section can produce several existing sections, including parabolic bottom-trapezoidal section [21], polygonal section with two sides [23], rectangular-above-trapezoidal section [24], section with two-segment linear sides, and HB [28]. These sections are obtained by setting $b_2 = b_3 = 0$ and specifying the appropriate conditions for b_1, z_f, z_2, and the polynomial parameters. It is interesting that other non-conventional shapes can also be generated from this versatile compound polynomial section.

Table 2. Special cases of compound and simple polynomial sections.

Polynomial Section Type	Special Section	Condition	Reference
Compound	Simple polynomial	$h_2 = f_2 = 0$	This paper
	Parabolic bottom- trapezoidal	$b_2 = b_3 = 0$, $b_1 = 0$, $b = d = 0$, $z_f = z_2$	Babaeyan et al. [21]
	Polygonal with two sides	$b_2 = b_3 = 0$, $b_1 = 0$, $c = d = 0$, $z_f > z_2$	Kurbanov and Khanov [23]
	Rectangular above trapezoidal	$b_2 = b_3 = 0$, $c = d = 0$, $z_2 = 0$	Abdulrahman [24]
	Two-segment linear sides with HB	$b_2 = b_3 = 0$, $c = d = 0$, $z_f > z_2$	Vatankhah [28]
Simple ($h_2 = f_2 = 0$)	Trapezoidal	$c = d = 0$	Chow [4]
	Rectangular	$c = d = z_f = 0$	Chow [4]
	Triangular	$c = d = b_1 = 0$	Chow [4]
	Parabolic sides without HB	$b = d = b_1 = 0$	Chow [4]
	Parabolic sides with HB	$b = d = 0$	Das [25]

The simple polynomial section generally has smooth corners at the bank level (called POLY-SM). For a certain condition of the polynomial parameters, the corners become sharp. Sharp corners occur before the inflection point of the third-degree polynomial. This condition is determined by equating the second derivative of y with respect to x, y'', to zero. Then, the following condition for sharp top corners is obtained.

$$B_f \geq -\frac{c}{3d} \tag{34}$$

The special cases of the simple polynomial section that have sharp top corners are trapezoidal ($c = d = 0$), rectangular ($c = d = z_f = 0$), triangular ($c = d = b_1 = 0$), parabolic without HB ($b = d = b_1 = 0$), and parabolic with HB ($b = d = 0$).

4. Optimization Model

4.1. Objective Function

The objective function of the optimization model for most economic section minimizes construction cost (excavation and lining) of the compound (or simple) polynomial section. Let λ be a binary variable defined as:

$$\lambda = \begin{cases} 1 \quad , & \text{for compound polynomial section} \\ 0 \quad , & \text{for simple polynomial section} \end{cases} \tag{35}$$

Then, the objective function can be written as:

$$\begin{aligned} \text{Minimize } C = c_1\Big[\lambda\big(A_{1f} + A_{2f} + A_{3f}\big) + (1-\lambda)\big(A_1 - h_2 T_{1f}\big)\Big] + c_2\left(2P_{sf}\right) \\ + c_3\Big\{\lambda\Big[2(\,h_2 + \,f_2)\sqrt{1+z_2^2}\Big]\Big\} + c_4[\lambda(\,b_2 + \,b_3) + \,b_1] \end{aligned} \tag{36}$$

where C = total construction cost per unit length of the channel, c_1 = per-area unit cost of section area, c_2 = cost per unit length of the side for subsection 1, c_3 = cost per unit length of the side for subsections 2 and 3, and c_4 = cost per unit length of the HB for subsection 1 and the banks for subsections 2 and 3. The term multiplied by c_1 is the section area that includes the freeboard. The terms multiplied by c_2 and c_3 are the length of the channel side that includes the freeboard for subsection 1, and subsections 2 and 3, respectively. The term multiplied by c_4 is the width of horizontal distance. As noted, for $\lambda = 1$, the term multiplied by c_1 will be the area of the compound polynomial section and for $\lambda = 0$ this term will be the area of the simple polynomial section, and similarly for other terms.

4.2. Design Discharge Constraint

Three methods for estimating the discharge were used in the optimization model: DCM (Equation (1)), E-AZ method (Equation (3)), and E-H method (Equation (5)). The discharge constraint is expressed as:

$$Q = \begin{cases} Q_{DCM}, & \text{(DCM)} \\ Q_{E\text{-}AZ}, & \text{(E-AZ Method)} \\ Q_{E\text{-}H}, & \text{(E-H Method)} \end{cases}, \quad (37)$$

where Q = design discharge (m^3/s).

4.3. Physical Constraints

A variety of physical constraints can be used in the model. Those include constraints on the physical output dimensions and possibly constraints on some decision variables. For example, constraints on the top section width may be specified as:

$$T_{1f} \leq T_{1f\ max} \quad (38)$$

$$T_{2f} \leq T_{2f\ max} \quad (39)$$

where $T_{1f\ max}$ and $T_{2f\ max}$ = maximum allowable widths of the compound section at the bank and ground levels, respectively. Clearly, a combination of physical constraints may be used.

4.4. Decision Variables, Input Data, and Model Solution

The decision variables of the optimization model are the polynomial parameters (b, c, and d), bottom width of the main channel b_1, inverse slope of the main channel side at the bank level z_f, floodplain water depth h_2, inverse side slope of the floodplain section z_2, and bank horizontal widths b_2 and b_3. The solution method requires as input the lower and upper bounds of each decision variable. The basic input data to the model are the design discharge Q, roughness coefficients (n_1 to n_4), construction unit costs (c_1 to c_4), longitudinal bed slope S_o, freeboards f_1 and f_2, binary variable λ, and any constraints on section dimensions.

The optimization model, which is nonlinear, was solved using Solver software that is available in Microsoft Excel [53]. The software implements the generalized reduced gradient method that uses multi-start strategy for global optimization. This method requires that lower and upper bounds on the decision variables be specified. In this strategy, candidate starting points are randomly generated within the specified bounds of the decision variables. Those points are then grouped into clusters and the software is run from a representative point in each cluster. As the process continues, clusters become smaller and capture each locally optimal solution, where a decision is then made to whether to continue the process. Ultimately, the software converges in probability to a globally optimal solution. Obviously, the model can be solved using other nonlinear optimization software.

4.5. Model Verification

Model verification was performed in two ways: Verifying the formulas of the compound section and verifying the optimization model for the simple polynomial section. For the compound section, the DEC discharge and roughness coefficient, Q_{DCM} and n_e, of Equations (1) and (2) of the numerical example of McAtee [50] were compared with those calculated in this study. The author's example involved a compound section with straight line sides for both the main channel and the floodplain subsections. Therefore, the parameters of the polynomial sides were set as $c = d = 0$ to obtain a trapezoidal main channel. The section was divided using vertical lines similarly to Figure 1. The author's input data were $b_1 = 15$ ft, $z_f = 5$, $b_2 = b_3 = 25$ ft, $z_2 = 0$, $h_1 = 3$ ft, and $h_2 = 2$ ft. The values of Q_{DCM} and n_e in this study were 848 ft^3/s and 0.031, which are identical to those of McAtee [50].

For the E-H method, the numerical example used by Hosseini [47] was used for comparison. The author's data were $b_1 = 1.1$ m, $z_f = 1.2$, $b_2 = b_3 = 4.03$ m, $z_2 = 0$, $h_1 = 1.2$ m, H = 2.8 m, and average $h_2 = 0.95$ m. In this example, the floodplain depth varies linearly from 1.6 m to 0.3 m. After making appropriate adjustments to maintain compatibility with the section in Figure 3, the values obtained in this study were $u = 0.869$, $v = 1.061$, $coh = 0.910$, $Q_{DCM} = 107.04$ m^3/s, and $Q_{E-H} = 99.54$ m^3/s, which are identical to those of Hosseini [47]. Note that in this example the DCM overestimates the discharge by 7.5%. As for the E-AZ method [46], there was no numerical example to be used for comparison.

For the simple polynomial section, it was reduced to a section with parabolic sides and a horizontal bottom (PSHB) by setting $b = d = 0$. Then, the model was verified by comparing the results of this special case with those of Das [25] who developed the PSHB section. The following input data of Das [25] were used: $Q = 100$ m^3/s, $S_o = 0.0016$, $n_1 = 0.015$, $n_2 = 0.018$, and 0.020 for the two sides, $c_1 = 0.6$, $c_2 = 0.1$ and 0.2 for the two sides, and $c_4 = 0.4$, where the unit costs are in Indian Rupees (IR). The case of fixed freeboard $f_1 = 0.5$ m was used. The comparison results of the simple polynomial and parabolic sections for C, h, b_1, z_f, and T_{1f} are presented in Table 3. As noted, the results are almost identical. The small differences occurred because Das [25] considered different side slopes (z_{1f} and z_{2f}) for the right and left sides, while in the simple polynomial section, the two side slopes were assumed equal (z_f).

Table 3. Comparison of minimum construction costs of the special case of simple polynomial section and parabolic sides and a horizontal bottom (PSHB) Section [1].

Variable	PSHB Section	Simple Polynomial Section ($b = d = 0$)
C (IR)	22.185	22.185
h (m)	4.700	4.699
b_1 (m)	2.415	2.416
z_{f1}	0.269	0.273
z_{f2}	0.278	0.273
T_{1f} (m)	8.103	8.101

[1] Input data are $Q = 100$ m^3/s, $c_1 = 0.6$, $c_2 = 0.1$ and 0.2 for the two sides, $c_4 = 0.4$, $f = 0.5$ m, $S_o = 0.0016$, $n_1 = 0.015$, and $n_2 = 0.018$ and 0.020 for the two sides.

5. Application

5.1. Example 1: Compound Polynomial Section

Consider a compound section with the input data shown in Table 4. The three methods of discharge prediction were used in the optimization model, one at a time, to design the optimal dimensions of the compound section. The decision variables (and their lower and upper bounds) were b_1 (1, 3), b (−3, 6), c (0, 6), and d (−0.1, −10). The constraint $0.3 \le (h_2/H) \le 0.45$ was also used.

Table 4. Input data for Examples 1 and 2.

Input Variable	Example 1 (Compound Section) [1]	Examples 2 and 3 (Simple Section)
n_1	0.013	0.015
n_2	0.013	0.020 (left), 0.018 (right)
n_3	0.016	n.a. [2]
n_4	0.016	n.a.
S_o (m/m)	0.0016	0.0016
Q (Q^3/s)	30	20
c_1 (IR)	0.6	0.6
c_2 (IR)	0.3	0.1 (left), 0.2 (right)
c_3 (IR)	0.3	n.a.
c_4 (IR)	0.2	0.4
f_1 (m)	0.3	0.5
f_2 (m)	0.3	n.a.
z_f	2 or 1	0.6 or 0.8 (for Ex. 2), 1000 (for Ex. 3)

[1] Other input data are $b_2 = b_3 = 1$ m and $z_2 = 0.5$. [2] n.a. = not applicable.

The optimal parameters corresponding to the three discharge methods are shown in Table 5a. As noted, the least cost corresponds to the DCM, while the largest cost corresponds to the E-H method. The discharges corresponding to the optimal design for each method are shown in Table 5b. The DCM predicts higher discharges, which are calculated as the sum of the three subsection discharges. This theoretical discharge was expected to be possibly greater than the discharge of the empirical methods, which are based on actual discharge measurements.

Table 5. Comparison of optimal results of the three discharge methods for the compound section.

Variable	DCM Method	E-AZ Method	E-H Method
(a) Optimal Dimensions			
C (IR)	9.007	9.813	9.861
b_1 (m)	2.03	2.99	2.05
b (m)	0.227	5.51	0.245
c (m)	4.244	0	4.256
d (m)	−3.387	−10	−2.832
h_2 (m)	0.95	0.80	0.80
h_1 (m)	1.16	1.57	1.66
T_{2f} (m)	6.88	6.90	7.09
(b) Discharges Corresponding to Optimal Dimensions			
Q_{DCM} (m^3/s)	30	33.4	34.5
$Q_{E\text{-}AZ}$ (m^3/s)	23.1 (−22.9% [1])	30 (−10.2%)	29.2 (−15.5)
Q_{E-H} (m^3/s)	25.2 (−16.1%)	29.0 (−13.1%)	30 (−13.1%)

[1] Percent difference from the DCM discharge value.

To illustrate, the discharge of the optimal section of the DCM (Table 5b) equals the design discharge (Q = 30 m^3/s) and the discharges corresponding to the E-AZ and E-H methods for that optimal section were 23.1 m^3/s and 25.2 m^3/s, respectively. Therefore, the optimal design based on the empirical methods would require larger dimensions and in turn larger costs than that of the DCM. The percentage deviations of the discharge of the empirical methods from the DCM are shown in Table 5b. As noted, there was no specific trend in the discharge prediction of the two empirical methods, where the discharge estimate of one method was sometimes greater or less than the other's estimate, depending on the geometry of the compound section. It is also noted that the percentage deviation ranged from −10.2% to −22.9%. Typically, a deviation of up to around 10% to 15% may be somehow tolerable due to the nature of the equations used. However, the deviation of the E-AZ method corresponding to the DCM as the design discharge constraint (−22.9%) lied outside the expected range. This large deviation maybe due to the uncertainness in the measurements, the empirical prediction of the discharges, the estimation of the roughness coefficient, and the best mode in which the Manning equation should be applied for compound sections. The optimal section corresponding to the E-AZ method, as an example, is shown in Figure 4a.

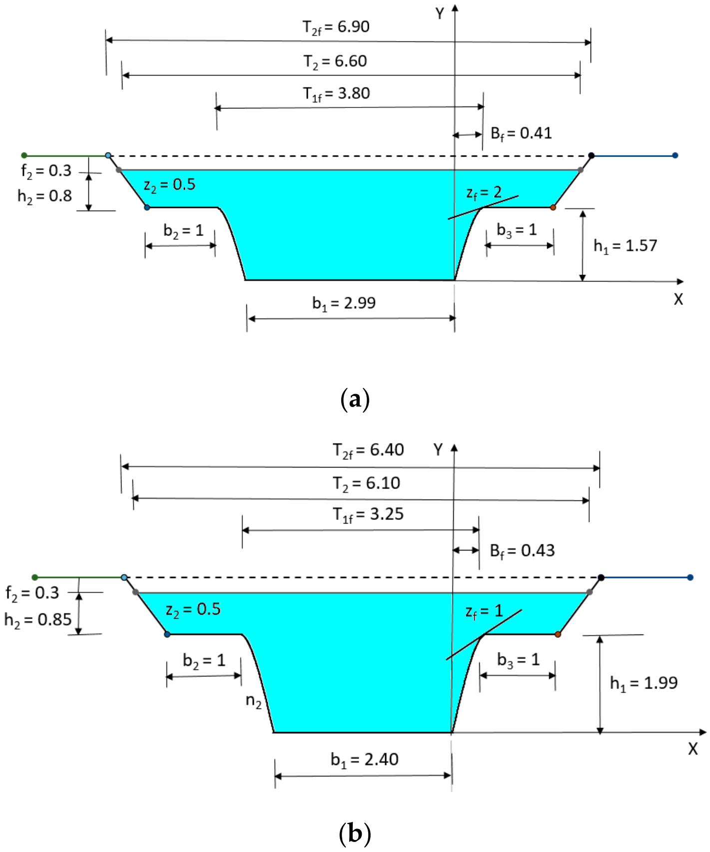

Figure 4. Optimal compound section corresponding to the E-AZ method (dimensions are in meters): (**a**) Restriction $z_f = 2$ and (**b**) restrictions $T_{2f} = 6.4$ m and $0.3 \leq (h_2/H) \leq 0.45$.

To illustrate the flexibility of the polynomial compound section, a constraint on the top width was used as $T_{2f} = 6.4$ m instead of the unconstrained value of 6.9 m obtained previously with the E-AZ Method. The variable z_f, with lower and upper bounds of 1 and 2, was considered as a decision variable to allow a feasible solution to be obtained. The optimal compound section is shown in Figure 4b. As noted, the bottom width b_1 was reduced to accommodate the constraint, while both h_1 and h_2 increased to satisfy the design discharge. The total cost slightly increased from 9.813 to 9.958 because the unit cost of the polynomial sides is greater than that of the horizontal bottom.

5.2. Example 2: Simple Polynomial Section

To compare the performance of the simple polynomial section with the PSHB section, different scenarios were used. For most scenarios, the POLY-SM and PSHB sections produced identical results (equally economical) since the parabolic section is a special case of the simple polynomial section. The only case where the simple polynomial section was more economical was when the section had a restricted side slope. This will be illustrated using a restricted inverse side slope $z_f = 0.6$ and 0.8. The input data for this example are shown in Table 4.

Consider Case 1 of Das [25], where the unit cost of the sides was less than that of the bottom. The optimal results of the simple polynomial and parabolic sections are presented in Table 6. As noted, the simple polynomial section was more economical than the parabolic section and the cost saving increased as the restricted inverse slope increased. For example, for z_f = 0.6 the total costs of the parabolic and simple polynomial sections were 22.991 and 22.516, respectively, indicating a cost saving by the POLY-SM section of 2.1%. For z_f = 0.8 the total costs of the parabolic and simple polynomial sections were 24.109 and 22.568, respectively, indicating a cost saving by the POLY-SM section of 6.4%. In Case 2, the unit costs of the sides were greater than the unit cost of the bottom. The comparison results are shown in Table 6 for only z_f = 0.6. As noted, the total costs of the parabolic and simple polynomial sections were 26.211 and 23.961, respectively, indicating that the cost saving by the POLY-SM section was 8.6%. Note also that the constraint on polynomial parameter b was binding at the lower bound (−1.000) and if this bound was relaxed, the cost saving would be even greater but the top corners of the sides would be less smooth.

Table 6. Optimal characteristics of simple polynomial section with smooth corners (POLY-SM) and parabolic section (PSHB) for restricted inverse side slope.

Item	Case 1 [1]				Case 2 [2] (z_f = 0.6)	
	z_f = 0.6		z_f = 0.8			
	PSHB	POLY-SM [3]	PSHB	POLY-SM [4]	PSHB	POLY-SM [5]
C (IR)	22.991	22.516	24.109	22.568	26.211	23.961
h (m)	4.15	4.57	3.62	4.53	3.21	3.53
b_1 (m)	0	3.37	0	3.83	3.35	6.06
z_f (left and right)	0.6	0.6	0.8	0.8	0.6	0.6
T_{1f} (m)	11.15	8.65	13.17	8.53	12.26	0.6
$A_{main\,f}$ (m^2)	34.54	32.37	36.17	32.24	34.51	9.46
P_{sf} (m)	7.57	5.82	8.03	5.65	6.05	32.01
A_{main} (m^2)	29.11	28.18	29.78	28.13	28.53	4.43
P_{main} (m)	13.96	13.88	14.77	13.96	14.27	27.41

[1] The side unit cost is less than the bottom unit cost: c_1 = 0.6, c_2 = 0.1 and 0.2, c_4 = 0.4. [2] The side unit cost is greater than the bottom unit cost (c_1 = 0.6, c_2 = 0.4 (for both sides), c_4 = 0.2). [3] Polynomial parameters: b = 0.0315, c = 1.5326, and d = −0.3091. [4] Polynomial parameters: b = 0.0, c = 2.2040, and d = −0.5501. [5] Polynomial parameters: b = 0.1936, c = 2.9825, and d = −1.000.

The optimal geometry of the parabolic and simple polynomial sections for Cases 1 and 2 (z_f = 0.6) are shown in Figure 5. Note that due to the larger unit cost of the bottom in Case 1, the parabollic section had no HB, but had resulted in considerably larger sides to satisfy the restricted slope. For Case 2, the parabolic section tried to use as long a bottom width as possible to minimize the total cost, but was unable to produce a larger width because of the side slope restriction. On the other hand, the simple polynomial section was able to use a larger bottom width and produce the required side slope because of the flexibility afforded by the extra parameter of the polynomial.

Another important advantage of the simple (or compound) polynomial section was that it could handle multiple constraints, such as restrictions on inverse side slope and total section width at the ground level. For example, for Case 1 and z_f = 0.8, the optimal PSHB section had T_{1f} = 13.17 m and horizontal bottom b_1 = 0 (Table 6). Therefore, if there was a constraint on the top width such that T_{1f} < 13.17 m, the parabolic section would have no feasible solution. On the contrary, under the same conditions, the simple polynomial section already had a feasible solution with T_{1f} = 8.53 m, as shown in Table 6. The flexibility of the simple polynomial section was due to the extra degree of freedom (extra parameter) of the third-degree polynomial.

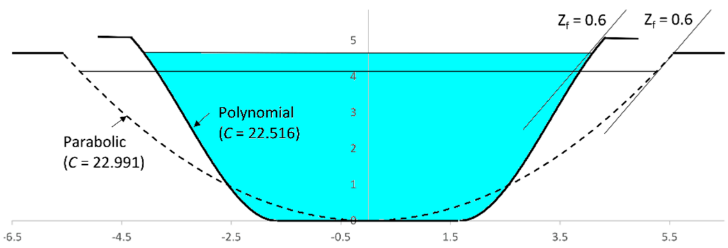

(**a**)

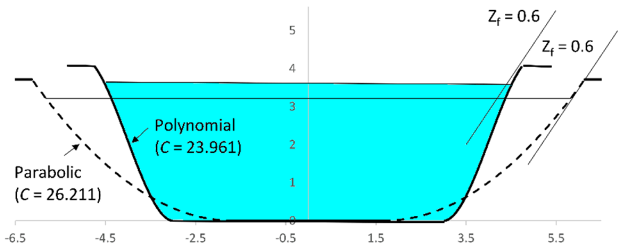

(**b**)

Figure 5. Comparison of simple polynomial section (POLY-SM) and parabolic section (PSHB) with restricted inverse side slope (z_f = 0.6): (**a**) Lining cost of sides is less than that of bottom (c_1 = 0.6, c_2 = 0.1 and 0.2, c_4 = 0.4) and (**b**) lining cost of sides is greater than that of bottom (c_1 = 0.6, c_2 = 0.4 for both sides, c_4 = 0.2).

5.3. Example 3: Simple Polynomial Section with $z_f = \infty$

To illustrate further the flexibility of the simple polynomial section, the data of Example 2 were used to develop the optimal section that had smooth top corners with a horizontal slope, where $z_f = \infty$ (very large value). The input data for this example are presented in Table 4. The decision variables (and their bounds) were b_1 (0, 3), b (0, 1), c (0, 5), and d (0,–2). The optimal section is shown in Figure 6. The optimal decision variables were b_1 = 1.74 m, b = 0.1465, c = 4, and d = −1.7463. Other section dimensions were h = 2.80 m, T_1 = 4.05 m, and T_{1f} = 4.81 m. The optimal cost was C = 8.252 IR.

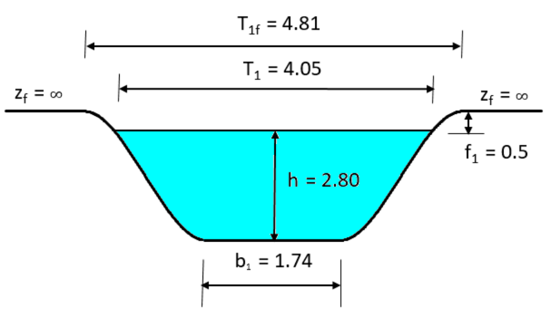

Figure 6. Optimal simple polynomial section with smooth top corners and horizontal slopes.at ground level ($z_f = \infty$; dimensions are in meters).

5.4. Sensitivity Analysis

A sensitivity analysis was conducted for the compound polynomial section to examine the sensitivity of the discharge and cost to small changes in the input variables. The variables were: (1) Roughness coefficients n_i, (2) longitudinal bed slope S_0, and (3) unit costs c_i, where i = 1 to 4. The analysis was performed using the data of Example 1 (Table 4) and the optimal dimensions of the compound section based on the E-AZ method. Each of the three preceding types of variables was changed one at a time by 10%, 20%, and 30%.

For the discharge sensitivity, the design discharge Q_{E-AZ} = 30 m^3/s was used as the base discharge. Using Equation (3), the calculated discharges corresponding to 10%, 20%, and 30% increase in n_i were −9.1%, −16.7%, and −23.1%, respectively. Those corresponding to S_0 were 4.9%, 9.5%, and 14.0%, respectively. Clearly, the discharge is more sensitive to the roughness coefficient than to the longitudinal bed slope. For the cost sensitivity, a change in the unit costs will result in identical change in the total cost since C is a linear function of c_i (Equation (36)). However, the effect of a change in the design discharge on the total cost will be different. Table 7 shows the change in the total cost due to different changes in the design discharge, along with other optimal variables. As noted, a 30% increase in the design discharge causes only 13.9% increase in the total cost. This moderate sensitivity of the cost to the design discharge is a useful finding, given the relatively large magnitude of error that is involved in the discharge prediction methods.

Table 7. Sensitivity of construction cost to changes in the design discharge.

Increase in Q (%)	Q (m^3/s)	C (IR)	Increase in C (%)	A_c (m^2)	P_c (m)	b_1 (m)
10	33	10.388	4.8	10.76	10.34	3.11
20	36	10.847	9.4	11.36	10.62	3.23
30	39	11.292	13.9	11.95	10.89	3.35

6. Concluding Remarks

This paper presented a new open channel compound section with third-degree polynomial sides for the main channel. The special case of no floodplains was also modeled as a simple polynomial section. The geometric and hydraulic characteristics of both polynomial-based sections were presented and an optimization model that minimized the construction cost for either section was presented. Based on this research, the following conclusions were made:

- The polynomial sides allow the top corners of the main channel sides to be smooth and this feature provided three advantages compared with conventional sharp corners: (1) The optimal construction cost of the section was reduced for the cases where there are restrictions on side slope and/or top section width, (2) smooth corners provide better maintenance than sharp corners and are less subject to erosion in the compound sections, and (3) smooth top corners of the simple polynomial sections provide better aesthetics.
- Given the challenge of estimating an accurate discharge of the compound section, care should be exercised in selecting a discharge constraint to be used in the optimization model. The conventional method, which assumes that the discharge is the sum of the subsection discharges, predicts higher discharges, and therefore could lead to inadequate design. In this study, two empirical methods for estimating section discharge were evaluated: One method is based on both field and laboratory experiments (E-AZ method) and the other is based on only laboratory experiments (E-H method). The results showed that there was no specific trend in the discharge prediction of the two empirical methods, where the discharge estimate of one method was sometimes greater or less than the other's estimate, depending on the geometry of the compound section. As such, either method may be used for estimating the discharge of compound channels.
- The compound polynomial section produced as special cases linear and parabolic sides of the main channel as well as several existing compound-like sections. In addition, the simple polynomial section produced as special cases other conventional sections such as trapezoidal and parabolic. The polynomial sides represent a useful contribution to the compound section that had always consisted of linear segments. The compound (or simple) polynomial section could be designed to minimize construction cost by considering different shapes of the sides and various types of physical constrains.

- The geometry of the compound polynomial section involved polynomial sides for only the main channel. The floodplain sides were assumed to be linear for simplicity. The purpose of adopting polynomial sides for the main channel was to provide a smooth transition between the main channel sides and the floodplain: (1) To reduce the effect of the erosion of the top corners of the main channel and (2) to improve aesthetic for the simple polynomial section. If necessary (e.g., as a result of side slope constraint), polynomial sides can also be used for the floodplain section. In this case, the compound section will consist of two simple polynomial sections on top of each other, which may simplify the analysis.
- This study showed that there was substantial difference between the discharges computed by the DCM and those predicted by the empirical methods. Further research should be conducted to develop more accurate empirical methods. Previous methods have focused on developing a single discharge formula using several dimensionless variables that have wide ranges of values. Accuracy may improve if the range of one (or more) critical variable is divided into subranges and a discharge formula is developed for each subrange. In addition, with respect to field and laboratory measurements, an analysis of experimental error and its propagation should be conducted as some variables may be not be fully controlled and the estimation of some parameters or coefficients required in the formulas (like roughness coefficient) may introduce important uncertainty in the analysis.
- An issue of compound channel hydraulics remains unresolved. In open channel sections (excluding closed ones), it is expected that the discharge increases when the flow depth increases. However, in compound channels, when the discharge is calculated in the transition from the lower to the upper trapezoidal section (considering the compound section as a single unit), it is well known that as the flow depth increases, the calculated discharge decreases abruptly and drastically. This occurs due to the great increase in the wetted perimeter, which is associated with a small increase in the flow area. Clearly, this is not logical and implies an error. The error increases when the roughness of the upper trapezoidal section is higher than that of the lower section. Future research to resolve this issue is needed.
- The results show that the simple polynomial section is more economical than the popular parabolic section for the cases of restricted side slope or top section width. In addition, the simple polynomial section is certainly more economical than the trapezoidal section, which has been shown in the literature to be inferior to the parabolic section. Since the polynomial side has an extra parameter, the new polynomial-based sections can handle multiple constraints, unlike the parabolic section. Given the important benefits provided by the new sections, they should be of interest to open channel designers.

Author Contributions: Conceptualization, S.M.E.; Formal Analysis, S.M.E.; Methodology, S.M.E. and Y.-C.H.; Writing—Original Draft, S.M.E.; Writing—Review & Editing, S.M.E. and Y.-C.H.

Funding: This research received no external funding.

Acknowledgments: The authors are grateful to three anonymous reviewers for their constructive and most helpful comments.

Conflicts of Interest: The authors declare no conflict of interest.

Notation

The following variables are used in this paper:

A_c	Flow area of the compound section
$A_{main\ f}$	Bank-full flow area of Subsection 1
A_{main}	Flow area of the simple polynomial section
A_1	Flow area of Subsection 1
A_{1f}	Total area of Subsection 1
A_2	Flow area of Subsection 2

A_{2f}	Total area of Subsection 2
A_3	Flow area of Subsection 3
A_{3f}	Total area of Subsection 3
B	Distance along water surface of the simple polynomial section from the y-axis to section side
B_f	Distance along bank level of the simple polynomial section from the y-axis to section side
b, c, d	Parameters of the third-degree polynomial
b_1	Width of HB of the main channel
b_2, b_3	Bank horizontal widths on the left and right sides of the compound section, respectively
C	Total construction cost per unit length of the channel
c_1	Per-area unit cost for section area
c_2	Cost per unit length of side for Subsection 1
c_3	Cost per unit length of side for Subsections 2 and 3
c_4	Cost per unit length of HB for Subsection 1 and banks of Subsections 2 and 3
u, v	Adjustment coefficients of Hosseini Method to improve the DCM discharges
coh	Coherence variable of the compound section
D_r	Ratio of water depth in the floodplain to that in the main channel
f_1, f_2	Freeboard of simple and compound polynomial sections, respectively
H	Water depth of the main channel
h	Water depth of the simple polynomial section
h_1	Bank-full water depth
h_2	Water depth in the floodplain subsections
K	Constant for a given polynomial
m	Number of wetted elements in the subsection
n_c	Composite Manning roughness coefficient
n_e	Equivalent Manning roughness coefficient based on Horton
n_i	Manning roughness coefficient of Subsection i
n_j	Roughness coefficient of element j of the subsection
n_1	Manning roughness coefficient of HB
n_2	Manning roughness coefficient of the main channel sides
n_3	Manning roughness coefficient of bank
n_4	Manning roughness coefficient of floodplain sides
N	Number of subsections of the compound section
P_i	Wetted perimeter of a Subsection i
P_j	Wetted length of element j of the subsection
P_c	Wetted perimeter of the compound section
P_{main}	Wetted perimeter of the simple polynomial section
P_s	Length of the wetted side of the simple polynomial section
P_{sf}	Length of the wetted side of Subsection 1
P_{main}	Wetted perimeter of the simple polynomial section
P_1	Wetted perimeter of Subsection 1
P_2	Wetted perimeter of Subsection 2
P_3	Wetted perimeter of Subsection 3
P_{2sf} , P_{3sf}	Lengths of the side of Subsections 2 and 3, respectively
Q	Design discharge
Q_{DCM}	Total discharge of the compound section based on divided channel method
Q_b	Bank-full discharge
Q_i	Discharge of subsection i
Q_t	Total discharge of the compound section based on the A-Z method
Q_1, Q_2, Q_3	Discharges of Subsections 1–3, respectively, using the DCM
Q_m, Q_f	Adjusted discharges of Subsection 1 and (2 and 3), respectively, using the DCM
R	Constant for a given polynomial
r^2	Coefficient of determination
S	Channel longitudinal bed slope
T_1	Width of the simple polynomial section at water surface
T_2	Width of the compound polynomial section at water surface
T_{1f}	Width of the main channel at the bank level

T_{2f}	Width of the compound polynomial section at ground surface
$T_{2f\ min}$	Minimum allowable widths of the compound section at the bank level
$T_{2f\ max}$	Maximum allowable widths of the compound section at the bank level
x, y	Cartesian coordinate axes
y'	First derivative of y with respect to x
y''	Second derivative of y with respect to x
z_f	Inverse side slope of the main channel at the ground level (horizontal to vertical)
z_2	Inverse side slope of the floodplain side slopes
λ	Binary variable (1 or 0 for compound or simple polynomial section)
θ	Constant for a given polynomial

References

1. Easa, S.M. *Open Channel Cross Section Design: Review of Recent Developments*; Chapter: 6, Advances in Measurements and Instrumentation: Reviews; Yurish, S.Y., Ed.; International Frequency Sensor Association Publishing: Barcelona, Spain, 2018; Volume 1, pp. 215–255.
2. Akan, A.O. *Open Channel Hydraulics*; Springer: New York, NY, USA, 2011.
3. Chaudhry, M.H. *Open Channel Flow*; Springer: New York, NY, USA, 2008.
4. Chow, V.T. *Open Channel Hydraulics*; McGraw-Hill: New York, NY, USA, 1959.
5. Swamee, P.K.; Bhatia, K.G. Economic open channel section. *Irrig. Power.* **1972**, *29*, 169–176.
6. Guo, C.; Hughes, W. Optimal channel cross section with freeboard. *J. Irrig. Drain. Eng.* **1984**, *110*, 304–314. [CrossRef]
7. Das, A. Optimal channel cross section with composite roughness. *J. Irrig. Drain. Eng.* **2000**, *126*, 68–72. [CrossRef]
8. Jain, A.; Bhattacharjya, R.K.; Sanaga, S. Optimal design of composite channels using genetic algorithm. *J. Irrig. Drain. Eng.* **2004**, *130*, 286–295. [CrossRef]
9. Aksoy, B.; Altan-Sakarya, A. Optimal lined channel design. *Can. J. Civ. Eng.* **2006**, *33*, 535–545. [CrossRef]
10. Han, Y.-C.; Easa, S.M.; Gao, X.-P. General explicit solutions of most economic sections and applications to trapezoidal and parabolic channels. *J. Hydrodyn.* **2018**. [CrossRef]
11. Froehlich, D.C. Width and depth-constrained best trapezoidal section. *J. Irrig. Drain. Eng.* **1994**, *120*, 828–835. [CrossRef]
12. Mironenko, A.P.; Willardson, L.S.; Jenab, S.A. Parabolic canal design and analysis. *J. Irrig. Drain. Eng.* **1984**, *110*, 241–246. [CrossRef]
13. Loganathan, G.V. Optimal design of parabolic canals. *J. Irrig. Drain. Eng.* **1991**, *117*, 716–735. [CrossRef]
14. Chahar, B.R.; Ahmed, N.; Godara, R. Optimal parabolic section with freeboard. *J Indian Water Works Assoc.* **2007**, 43–48.
15. Hussein, A.S. Simplified design of hydraulically efficient power-law channels with freeboard. *J. Irrig. Drain. Eng.* **2008**, *134*, 380–386. [CrossRef]
16. Strelkoff, T.S.; Clemmens, A.J. Approximating wetted perimeter in power-law cross section. *J. Irrig. Drain. Eng.* **2000**, *126*, 98–109. [CrossRef]
17. Anwar, A.A.; Clarke, D. Design of hydraulically efficient power-law channels with freeboard. *J. Irrig. Drain. Eng.* **2005**, *131*, 560–563. [CrossRef]
18. Anwar, A.A.; de Vries, T.T. Hydraulically efficient power law channels. *J. Irrig. Drain. Eng.* **2003**, *129*, 18–26. [CrossRef]
19. Carson, H.; Kingman, H.; Haynes, T.; Collison, H.N. Cross-sections of sewers and diagrams showing hydraulic elements of four general types, Metropolitan Sewerage Systems. *Eng. News* **1894**, *30*, 121–123.
20. Diogo, A.F.; Barros, L.T.; Santos, J.; Temido, J.S. An effective and comprehensive model for optimal rehabilitation of separate sanitary sewer systems. *Sci. Total Environ.* **2018**, *612*, 1042–1057. [CrossRef] [PubMed]
21. Babaeyan-Koopaei, K.; Valentine, E.M.; Swailes, D.C. Optimal design of parabolic-bottomed triangle canals. *J. Irrig. Drain. Eng.* **2000**, *126*, 408–411. [CrossRef]
22. Chahar, B.R.; Basu, S. Optimal design of curved bed trapezoidal canal sections. *Water Manag.* **2009**, *162*, 233–240. [CrossRef]

23. Kurbanov, S.O.; Khanov, N.V. A hydraulic analysis of the most efficient section of a power engineering channel with a polygonal profile. *Power Tech. Eng.* **2003**, *37*, 213–216.
24. Abdulrahman, A. Best hydraulic section of a composite channel. *J. Hydraul. Eng.* **2007**, *133*, 695–697. [CrossRef]
25. Das, A. Optimal design of channel having horizontal bottom and parabolic sides. *J. Irrig. Drain Eng.* **2007**, *133*, 192–197. [CrossRef]
26. Froehlich, D.C. Most hydraulically efficient standard lined canal sections. *J. Irrig. Drain Eng.* **2008**, *134*, 462–470. [CrossRef]
27. Easa, S.M. Improved channel cross section with two-segment parabolic sides and horizontal bottom. *J. Irrig. Drain. Eng.* **2009**, *135*, 357–365. [CrossRef]
28. Vatankhah, A.R. Semi-regular polygon as the best hydraulic section in practice (generalized solutions). *Flow Meas. Instrum.* **2014**, *38*, 67–71. [CrossRef]
29. Easa, S.M. New and improved channel cross section with piece-wise linear or smooth sides. *Can. J. Civ. Eng.* **2011**, *38*, 690–697. [CrossRef]
30. Easa, S.M.; Vatankhah, A.R. New open channel with elliptic sides and horizontal bottom. *KSCE J. Civ. Eng.* **2014**, *18*, 1197–1204. [CrossRef]
31. Easa, S.M. Versatile general elliptic open channel cross section. *KSCE J. Civ. Eng.* **2016**, *20*, 1572–1581. [CrossRef]
32. Han, Y.-C.; Easa, S.M. Superior cubic channel section and analytical solution of best hydraulic properties. *Flow Meas. Instrum.* **2016**, *50*, 169–177. [CrossRef]
33. Han, Y.-C.; Easa, S.M. Exact solution of optimum hydraulic power-law section with general exponent parameter. *J. Irrig. Drain. Eng.* **2018**, *44*, 04018035. [CrossRef]
34. Posey, C.J. Computation of discharge including over-bank flow. *Civ. Eng.* **1967**, *37*, 62–63.
35. Shiono, K.; Knight, D.W. Two-dimensional analytical solution for a compound channel. In Proceedings of the 3rd International Symposium on Refined Flow Modeling and Turbulence Measurements, Tokyo, Japan, 26–28 July 1988; pp. 503–510.
36. Wark, J.B.; Samuels, P.G.; Ervine, D.A. A practical method of estimating velocity and discharge in compound channels. In Proceedings of the International Conference on River Flood Hydraulics, London, UK, 17–20 September 1990; pp. 163–172.
37. Ackers, P. Hydraulic design of two-stage channels. *J. Water Marit. Eng.* **1992**, *96*, 247–257.
38. Wormleaton, P.R.; Merrett, D.J. An improved method of calculation for steady uniform flow in prismatic main channel/flood plain sections. *J. Hydraul. Res.* **1990**, *28*, 157–174. [CrossRef]
39. Lambert, M.F.; Myers, R.C. Estimating the discharge capacity in straight compound channels. *Water Marit. Energy* **1998**, *130*, 84–94. [CrossRef]
40. Bousmar, D.; Zech, Y. Momentum transfer for practical flow computation in compound channels. *J. Hydraul. Eng.* **1999**, *125*, 670–696. [CrossRef]
41. Ervine, D.A.; Babaeyan-Koopaei, K.; Sellin, R.H. Two-dimensional solution for straight and meandering overbank flows. *J. Hydraul. Eng.* **2000**, *126*, 653–669. [CrossRef]
42. MacLeod, A.B. Development of Methods to Predict the Discharge Capacity in Model and Prototype Meandering Compound Channels. Ph.D. Thesis, University of Glasgow, Glasgow, UK, 1997.
43. Liu, W.; James, C.S. Estimation of discharge capacity in meandering compound channels using artificial neural networks. *Can. J. Civ. Eng.* **2000**, *27*, 297–308. [CrossRef]
44. Zahiri, A.; Dehghani, A.A. Flow discharge determination in straight compound channels using ANN. *World Acad. Sci. Eng. Technol.* **2009**, *58*, 1–8.
45. Unal, B.; Mamak, M.; Seckin, G.; Cobaner, M. Comparison of an ANN approach with 1-D and 2-D methods for estimating discharge capacity of straight compound channels. *Adv. Eng. Softw.* **2010**, *41*, 120–129. [CrossRef]
46. Azamathulla, H.; Zahiri, A.R. Flow discharge prediction in compound channels using linear genetic programming. *J. Hydrol.* **2012**, *454–455*, 203–207. [CrossRef]
47. Hosseini, S.M. Equations for discharge calculation in compound channels having homogenous roughness. *Iran. J. Sci. Technol. Trans. B* **2004**, *28*, 537–546.
48. Fernandes, J.N.; Leal, J.B.; Cardoso, A.H. Flow structure in a compound channel with smooth and rough floodplains. *Eur. Water* **2012**, *38*, 3–12.

49. Horton, R.E. Separate roughness coefficients for channel bottom and sides. *Eng. News Rec.* **1933**, *111*, 652–653.
50. McAtee, K. Introduction to Compound Channel Flow Analysis for Floodplains. Online Continuing Education for Engineers, SunCam. 2019. Available online: www.SunCam.com (accessed on 25 April 2019).
51. Motayed, A.K.; Krishnamurthy, M. Composite roughness of natural channels. *J. Hydraul. Div.* **1980**, *106*, 1111–1116.
52. Yang, K.; Cao, S.; Liu, X. Flow resistance and its prediction methods in compound channels. *Acta Mech. Sin.* **2007**, *1*, 23–31. [CrossRef]
53. Microsoft. Microsoft Excel 2010 User Guide. Available online: https://www.ncl.ac.uk/ltds/assets/documents/Excel-AnalysingDataUsingFormulaePivotTables.pdf (accessed on 28 April 2019).